

Thermal photons as a sensitive probe of α -cluster in C+Au collisions at the BNL Relativistic Heavy Ion Collider

Pingal Dasgupta,¹ Guo-Liang Ma,^{1,*} Rupa Chatterjee,^{2,†} Li Yan,^{1,‡} Song Zhang,¹ and Yu-Gang Ma^{1,§}

¹*Key Laboratory of Nuclear Physics and Ion-beam Application (MOE),
Institute of Modern Physics, Fudan University, Shanghai 200433, China*

²*Variable Energy Cyclotron Centre, HBNI, 1/AF, Bidhan Nagar, Kolkata-700064, India*

Different orientations of α -clustered carbon nuclei colliding with heavy ions can result in a large variation in the value of anisotropic flow. Thus, photon flow observables from clustered ^{12}C and ^{197}Au collisions could be a potential probe to study the ‘direct photon puzzle’. We calculate the transverse momentum spectra and anisotropic flow coefficients (v_n) of thermal photons from collisions of triangular α -clustered carbon and gold at $\sqrt{s_{\text{NN}}} = 200$ GeV at RHIC using a hydrodynamic model framework and compare the results with those obtained from unclustered carbon and gold collisions. The slope of the thermal photon spectra is found to vary moderately for different orientations of collisions. However, we find that the elliptic (v_2) and triangular flow (v_3) coefficients of direct photons for specific configurations are significantly larger and predominantly formed by the QGP radiation. A strong anti-correlation between initial spatial ellipticity and triangularity is observed in an event-by-event framework of α -clustered C + Au collisions. These special features provide us an opportunity to detect the exotic nature of cluster structure inside carbon nucleus using the photon probe in the future experiments.

I. INTRODUCTION

The experimental study of relativistic heavy-ion collisions provides a strong evidence of the formation of hot and dense Quark-Gluon Plasma (QGP) state of matter at the center of the collision zone [1–5]. The relativistic hydrodynamic models present a satisfactory description of fireball evolution as the copious production and large harmonic flow of hadrons have been successfully explained by these frameworks [6–19]. The past studies have shown that nuclear deformation can be investigated from the anisotropic flow of produced hadrons at intermediate and high collision energies [20–23]. The nuclear collisions at such energies provide us a unique way to investigate the intrinsic substructure of nuclei as the time during which the participating nuclei pass through each other is too small for any slower nuclear excitation to occur and thus one can obtain a projection of overlying nuclear distributions on the fireball.

For example, the small systems, such as p + p and p + A have gathered much attention for producing anisotropic flow coefficients comparable to the peripheral heavy ion collisions in recent times [24]. The measurements of p + Au, d + Au, and ^3He + Au collisions at 200A GeV have clearly shown the footprints of initial geometries (initial ellipticity and triangularity) on the anisotropic flow coefficients [25]. The successful hydrodynamical description of those data has strongly suggested that the initial nucleon-level geometries have been transferred into the momentum anisotropies through hy-

drodynamical evolution of small droplets of the QGP in these small systems.

An analogous initial geometry effect of nuclei is also found to be present in the intermediate energy heavy-ion collisions however at a cluster level [26, 27]. A few recent articles have argued that the geometric α -clustering structure of light nuclei can be realized in the realm of relativistic collisions [28–30]. Gamow first proposed the possibility of clustered states in light nuclei [31]. The identification of the fusion reaction mechanism for carbon production has led to the discovery of the clustered states [32, 33]. However, many theoretical models such as no-core shell model [34], fermionic molecular dynamics [35], the variational Green’s function [36], Bose-Einstein Condensate (BEC) [37–39], etc. have not been successful in explaining such clustered structures of nuclei. The α -clustering inside a light nucleus produces nuclear deformity and spatial correlations between clusters. It has been suggested that α -clustering configurations can be identified by giant dipole resonance [40, 41] or photonuclear reactions [42–44]. The strategy of investigating initial nucleon-level geometry via measuring flow in a relativistic heavy-ion collision has a great potential to identify the geometric structures of clustered nuclei [28, 30, 45, 46].

On the other hand, the direct photons are considered as one of the efficient probes to study the properties of hot and dense QGP state of matter [47–61]. The thermal photon spectra obtained from the hydrodynamical model evolution combined with the prompt photon contribution from initial partonic hard scatterings have satisfactorily described the measured direct photon spectra in the range $p_T > 2$ GeV in heavy-ion collisions at both Relativistic Heavy Ion Collider (RHIC) and the Large Hadron Collider (LHC). The theoretical calculation of spectra in the region $p_T < 2$ GeV has, however, been found to underestimate the data where the contribution from the

*glma@fudan.edu.cn

†rupa@vecc.gov.in

‡cliyan@fudan.edu.cn

§mayugang@fudan.edu.cn

hadronic phase is significant. The anisotropic flow of direct photons is also believed to be a potential probe for illustrating the initial state of a collision. However, the hydrodynamic model calculations of photon production failed to describe the elliptic and triangular flow data at RHIC and LHC by a large margin, which has been addressed as the “direct photon puzzle” [62, 63]. Several studies using a more realistic hydrodynamic framework, initial conditions, the pre-equilibrium flow, and holographic thermal-photon emission rate have shown improvements in the theoretical prediction but could not resolve the puzzle yet [64–67]. Recent studies have shown that the spectra and anisotropic flow coefficients of photons (i.e., v_1, v_2, v_3) from different collision systems and their simultaneous comparison could be valuable to understand the sources of the puzzle [68–70]. A significant improvement in the photon anisotropic flow has been reported recently by Naboka *et al.* using integrated hydrokinetic model [71, 72].

In the present article, we aim to study the intrinsic geometry of the α -clustered C nucleus using the photon probe. We calculate the spectra and anisotropic flow coefficients v_n ($n = 2, 3$) of thermal photons in (2+1) dimensional inviscid hydrodynamic framework from the α -clustered C + Au collisions at the center-of-mass energy $\sqrt{s_{NN}}=200$ GeV. The same set of observables from the unclustered C + Au collisions (see Section II) is also calculated for comparison.

This paper is organized as follows. In the next section, we briefly discuss the initial parameters and the framework for the model calculation. In section III we present how initial spatial anisotropies ε_n and the momentum anisotropies of thermal photons v_n are calculated. In section IV we discuss the results of thermal photon spectra and anisotropic flow coefficients and finally, we summarize our results in section V.

II. INITIAL CONDITION AND HYDRODYNAMIC FRAMEWORK

In the present work, we adapt the same procedures followed in [30] to choose the initial parameters for the nuclear density distribution of α -clustered carbon. We study different collision scenarios incorporating two types of carbon nucleus in the Monte Carlo Glauber (MCG) framework :

- **α -clustered carbon:** This is an equilateral triangle shaped α -clustered state of carbon. It is considered as the ground state of clustered phase with binding energy 7.17 MeV/nucleon. There exists another possible excited state of the clustered structure, a chain-like structure of 3 alpha particles with binding energy 7.47 MeV/nucleon. However, in this article, we emphasize only on the triangle shaped carbon. We use a parametric form of nucleon distribution function for each α cluster [30] and centers

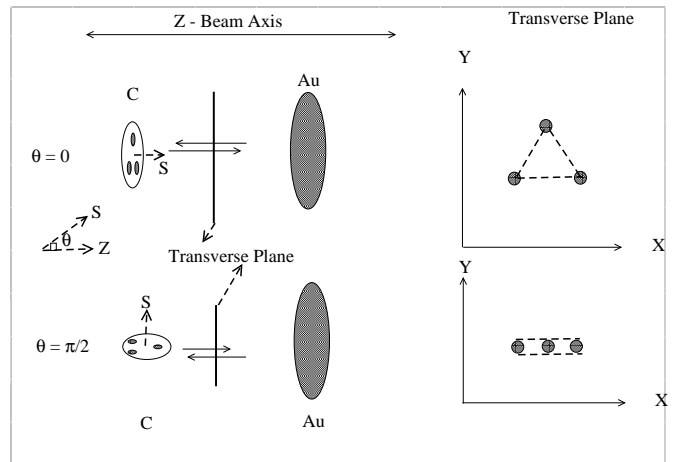


FIG. 1: A schematic view of collisions of the α -clustered carbon with a gold nucleus. The different orientations of clustered-carbon at the time of impact lead to different initial geometries (left). The triangular and line geometry appear when clustered carbon hits the gold wall with an angle 0 and $\pi/2$ respectively (right). The angle is measured between the beam axis (z -axis) and the perpendicular axis of the triangular carbon nucleus in $z - y$ plane.

of such three α clusters are placed on the vertices of an equilateral triangle. The parameters are fixed in such a manner that one-body radial density distribution of the center of nucleons obeys the results of the BEC model [39]. The distribution of nucleons in each cluster is expressed through a Gaussian function as follows :

$$f_i(\vec{r}) = A \exp\left(-\frac{3}{2}(\vec{r} - \vec{c}_i)^2/r_\alpha^2\right), \quad (1)$$

where, \vec{c}_i represents the center of the i^{th} cluster. r_α determines the mean radius of each cluster. We generate positions of nucleons in each alpha cluster from the above distribution function and then shift three of such clusters to the vertices of a triangle of length l . The short distance repulsion of nucleons is also an essential criterion for light nuclei, where the distance between two centers of an N-N pair cannot be less than 0.9 fm [30]. The nucleonic positions are finally shifted to a new coordinated system where the center-of-mass resides on the origin. The parameters l and r_α in Eq.(1) are taken as 3.05 fm and 0.96 fm respectively to match the results from BEC model calculations [30].

- **Unclustered carbon:** This is a mean-field state of C nucleus. The nuclear distribution is isotropic for this case. A two-parameter Wood-Saxon distribution of nuclear density is considered for an unclustered carbon where the parameters are adjusted in such a way that the root mean square radius of the nuclear distribution remains the same as the clustered carbon (~ 2.26 fm).

To distribute the nucleons inside a gold nucleus we employ the standard two-parameter Wood-Saxon nuclear density distribution profile. We assume that the beam axis is stretched along the z -direction and the impact parameter lies along the x -direction in each event of the collision.

The conventional two-component MCG technique is then used to distribute initial entropy density on the transverse plane. The criterion for a collision between the two incoming nucleons is made as $d^2 < \frac{\sigma_{NN}}{\pi}$, where d is the transverse distance between the colliding nucleons and σ_{NN} is the inelastic nucleon-nucleon cross-section which at RHIC is about 42 mb. A participant is given a weight of $(1 - \nu)$ and a binary collision is given a weight of ν , where ν is taken as 0.145 [30]. The entropy density distribution, $s(x, y)$, is obtained by taking a weighted sum over all the sources as explained in Eq.(2) below.

$$s(x, y) = K \sum_{i,j=1}^{N_{\text{part}}, N_{\text{coll}}} [\nu n_{\text{coll}}(x_i, y_i) f_i(x, y) + (1 - \nu) n_{\text{part}}(x_j, y_j) f_j(x, y)], \quad (2)$$

where, n_{part} and n_{coll} denote the number of participant and binary collision sources at the (x, y) position respectively. K is a normalization factor which decides the total multiplicity of an event. The function $f_{i,j}(x, y)$ is a normalized distribution of the following form centering about the i^{th} collision or j^{th} participant source :

$$f_{i,j}(x, y) = \frac{1}{2\pi\sigma^2} e^{-\frac{(x-x_{i,j})^2 + (y-y_{i,j})^2}{2\sigma^2}}. \quad (3)$$

The initial entropy density profile which serves as an input for our hydrodynamic calculation is obtained by taking an initial state average of 10000 events with random nucleonic positions at impact parameter $b \approx 0$ fm. We modify the (2+1) dimensional ideal relativistic hydrodynamic model [14] to obtain the space-time evolution of the above initial entropy distribution at the mid-rapidity. The initial flow velocity component, v_x and v_y are taken as zero. For the sake of simplicity, we take the value of initial thermalization time as $\tau_0 = 0.17$ fm/c which has been used for the Au + Au collisions at RHIC [68, 73], although one may expect a larger value of initial thermalization time for small systems. A lattice-based equation of state [74] is used and we consider a constant temperature freeze-out at 160 MeV. The same freeze-out temperature (T_f) is used in earlier studies of Au+Au collisions at RHIC using the same hydrodynamical model [49, 64, 68, 70].

III. ANISOTROPIC FLOW OF THERMAL PHOTONS

The production of thermal photons from the quark gluon plasma phase is estimated by using the complete next-to-leading order photon rates from Refs. [75, 76].

We use the parameterized rates from Ref. [77] to calculate the photon production from the hot hadronic matter phase. The emission rates ($R = EdN/d^3p d^4x$) from QGP and hadronic matter phases are integrated over the space-time history to estimate the total thermal production and anisotropic flow. The flow coefficients v_n are calculated as:

$$v_n(p_T) = \frac{\int_0^{2\pi} d\phi \cos[n(\phi - \psi_n)] \frac{dN}{p_T dp_T dy d\phi}}{\int_0^{2\pi} d\phi \frac{dN}{p_T dp_T dy d\phi}}, \quad (4)$$

where ϕ is the azimuthal angle of particle's momentum and the event plane angle ψ_n is determined by,

$$\psi_n = \frac{1}{n} \arctan \frac{\int dx dy r^2 \sin(n\Phi) \epsilon(x, y, \tau_0)}{\int dx dy r^2 \cos(n\Phi) \epsilon(x, y, \tau_0)} + \pi/n, \quad (5)$$

where $\epsilon(x, y, \tau_0)$ is the energy density at an initial proper time τ_0 at (x, y) point on the transverse plane, Φ and r are the spatial azimuthal angle and radial distance. The corresponding initial state anisotropy ϵ_n is quantified as [68, 70, 78]:

$$\epsilon_n = -\frac{\int dx dy r^2 \cos[n(\Phi - \psi_n)] \epsilon(x, y, \tau_0)}{\int dx dy r^2 \epsilon(x, y, \tau_0)}. \quad (6)$$

IV. RESULTS AND DISCUSSIONS

A. Initial configurations

We consider three typical configurations of collisions, i.e., $\theta = 0, \pi/4$, and $\pi/2$ in this study. This can be imagined as a deformed nucleus hitting a wall of a gold nucleus at different orientation angles (see Fig. 1). Thus, the angle $\theta = 0$ describes situation where the symmetry axis is aligned with the beam axis producing an initial triangular geometry in the deposited entropy distribution and the highest multiplicity amongst all orientations of collision. For $\theta = \pi/2$, the multiplicity is the lowest. While a triangular geometry vanishes for such a scenario, a large elliptic geometry appears. We consider an intermediate situation where the symmetry axis makes an angle $\pi/4$ with the beam axis producing both the intrinsic elliptic and triangular geometry in the deposited entropy distribution.

In Fig. 2 (a), (b), and (c) the event-averaged initial entropy density profile for three orientation angles 0, $\pi/4$, and $\pi/2$ are shown respectively, while Fig. 2(d) represents the entropy profile for the unclustered carbon. We see that the entropy density at the center of each hot spot region for the clustered case is much larger than the entropy density obtained at the center of the unclustered case. In Fig. 2(a) and (b), the entropy profiles are seen to have a triangular shape, while in Fig. 2(c) a peanut-like structure appears with no such triangular geometry. The triangular eccentricity (ϵ_3) of the initial entropy density distribution for the cases in Fig. 2(a) and (b) is 0.43 and

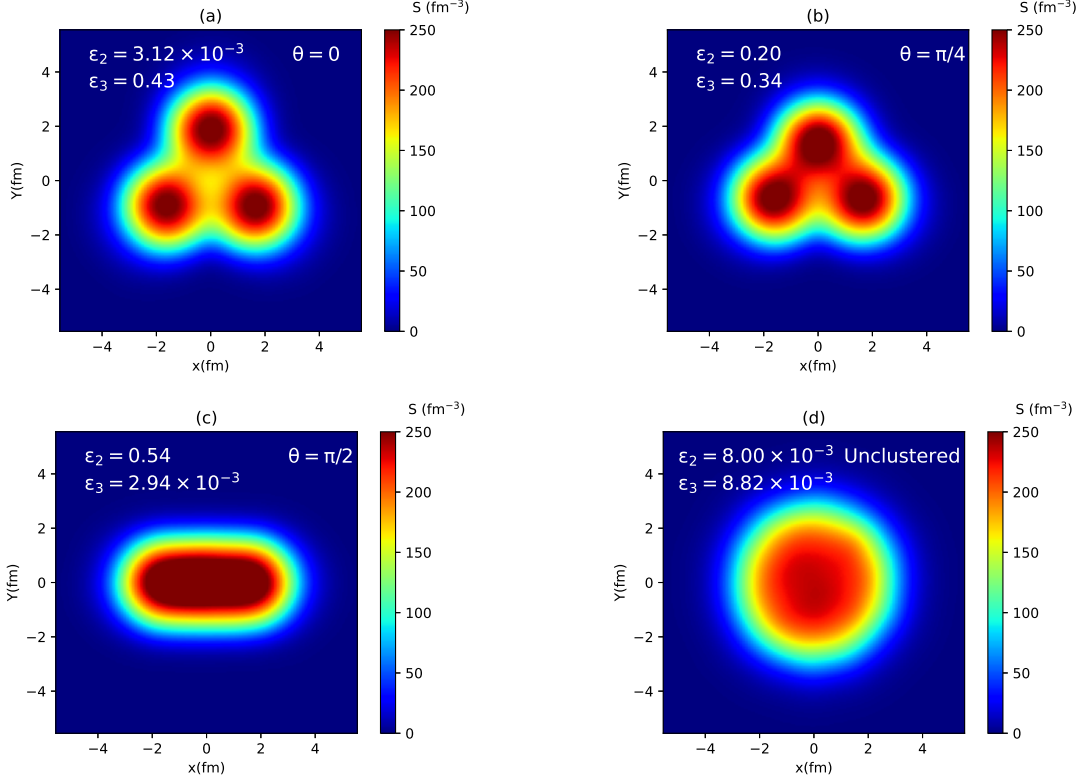


FIG. 2: (Color online) Distribution of entropy density at the formation time τ_0 on transverse ($x-y$) plane for central ($b \approx 0$ fm) C + Au collisions at 200A GeV. The figures (a), (b), and (c) correspond to the collisions of clustered C and Au at angles $0, \pi/4$ and $\pi/2$ respectively, whereas, (d) represents the initial entropy profile from collision of unclustered C and Au.

0.34 respectively. On the other hand, the elliptic eccentricity (ε_2) for the cases in Figs. 2(b) and (c) is 0.20 and 0.54 respectively, whereas ε_2 is vanishingly small for the other two cases.

B. Evolution of temperature and flow velocity

The time evolution of average temperature $\langle T \rangle$ and average transverse flow velocity $\langle v_T \rangle$ for the three configurations of collision for the clustered carbon and the unclustered carbon is shown in Fig. 3(a) and (b) respectively. The $\langle T \rangle$ and $\langle v_T \rangle$ are obtained by Eq. (7) and Eq. (8), respectively, i.e.

$$\langle T \rangle = \frac{\int dx dy T(x, y, \tau) \epsilon(x, y, \tau)}{\int dx dy \epsilon(x, y, \tau)}, \quad (7)$$

$$\langle v_T \rangle = \frac{\int dx dy v_T(x, y, \tau) \epsilon(x, y, \tau)}{\int dx dy \epsilon(x, y, \tau)}. \quad (8)$$

The initial average temperature (see Fig. 3 (a)) is found to be largest (~ 440 MeV) for the configuration $\theta = \pi/2$ and smallest for the unclustered case (~ 407 MeV). A relatively smaller area of the overlapping region leads to

a larger $\langle T \rangle$ for the configuration $\theta = \pi/2$ at the initial time. We see an almost similar time evolution of the average temperature for all the configurations. However, the evolution of the average transverse flow velocity for different configurations are distinct from each other (see Fig. 3(b)). We see that $\langle v_T \rangle$ sharply rises for the clustered cases, whereas the rise is relatively slower for the unclustered case. The rise is maximum for the orientation angle $\pi/2$. During the time interval of $2 < \tau < 4$ fm/c, we observe a sudden jerk for the configuration $\theta = 0$. However, no such effect is found for $\theta = \pi/4$ and $\pi/2$. The radially outward ripples, originated at the boundary of each hotspot (see Fig. 2 (a)), cause a flow cancellation when they collide, which effectively reduces the growth of the average transverse flow velocity.

C. Spectra and anisotropic flow

In Fig. 4, the thermal photon spectra are presented for the clustered and unclustered C + Au collisions. The thermal photon spectra for all the cases are found to be almost similar in the region $p_T < 2$ GeV. However, the spectra become sensitive to the orientation angle for $p_T > 2$ GeV. The thermal spectrum for the configuration $\theta = \pi/2$ is found to be slightly above the other spectra in the larger p_T region. On the other hand, photon produc-

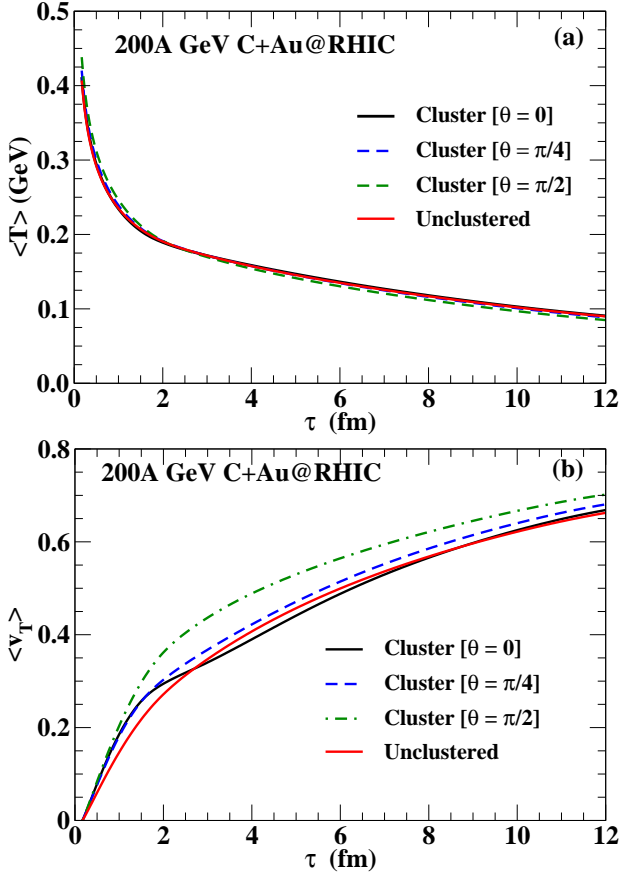


FIG. 3: (Color online) (a) Time evolution of average temperature and (b) transverse flow velocity for different configurations of clustered C and Au collisions at 200A GeV. The same variables for the collisions of unclustered C and Au are shown for a comparison.

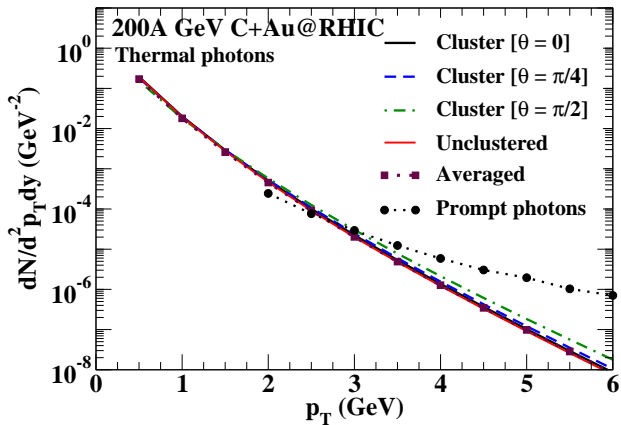


FIG. 4: Thermal photon spectra for different configurations of clustered C and Au collisions at 200A GeV. The thermal photons from the collisions of unclustered C and Au are shown for a comparison.

tion from the unclustered carbon is found to be smallest. We plot a thermal photon spectrum (i.e. maroon box+dotted line) considering an orientation-averaged initial profile (averaged over 50,000 events with random orientations) for the clustered carbon and find it similar to the spectrum obtained for the unclustered carbon. We estimate the prompt photon production in the region $p_T > 2$ GeV from C + Au collisions by scaling the prompt photon spectrum obtained in the p+p collisions at 200A GeV using the Monte Carlo code JETPHOX (version 1.2.2) [79]. We expect similar production of prompt photons for collisions of clustered as well as unclustered carbon as the N_{coll} for both are close to each other. The Fig. 4 shows the prompt photons contribute significantly in the region $p_T > 3$ GeV (black filled circles).

The elliptic and triangular flow of thermal photons as a function of p_T are presented in Fig. 5(a) and (b) respectively. We see a substantially large thermal photon v_3 for the configurations $\theta = \pi/4$ and $\theta = 0$. The initial triangular geometry of the entropy density profile produced in the collision of α -clustered carbon and gold nucleus gives rise to the triangular flow of thermal photons. As there exists no such triangular geometry for the configuration $\theta = \pi/2$ or the unclustered case, we obtain a vanishingly small thermal photon v_3 . The thermal photon v_3 for the configuration $\theta = \pi/4$ is seen to be slightly larger compared to the same obtained from the orientation angle $\theta = 0$ even though the triangular anisotropy is smaller for the former than the latter. The reason is attributed to the larger average transverse flow velocity during the evolution for the configuration $\theta = \pi/4$ than the same obtained for the configuration $\theta = 0$. On the other hand, the elliptic flow parameter of thermal photons is found to be vanishingly small for the configuration $\theta = 0$ and the unclustered case. However, the thermal photon v_2 is found to be very large for the orientation angle $\pi/2$. The initial elliptic eccentricity and the transverse flow velocity, both play significant role in producing a large v_2 of thermal photons for the configuration $\theta = \pi/2$. It is important to note that the v_2 obtained for the above configuration is comparable to the direct photon v_2 data obtained for the mid-central Au+Au collisions at 200A GeV at RHIC [62].

To obtain a more precise idea about the origin of the anisotropic flow coefficients of photons, we plot the individual contributions from the QGP and hadronic phases to the total value of the flow coefficients in Fig 6. We calculate the contributions of thermal photon v_3 for the clustered case with orientation angles $\theta = 0$ and $\pi/4$ in Fig 6(a). We find that the maximum value of v_3 (at $p_T \sim 2$ GeV) from the QGP phase is substantial and close to the maximum value of the total thermal photon v_3 . Hence, the response to the initial-state triangular geometry is predominantly carried by the QGP evolution. If we compare the hadronic medium contribution to the total thermal photon v_3 for these cases, we find that unlike the QGP photon v_3 , the

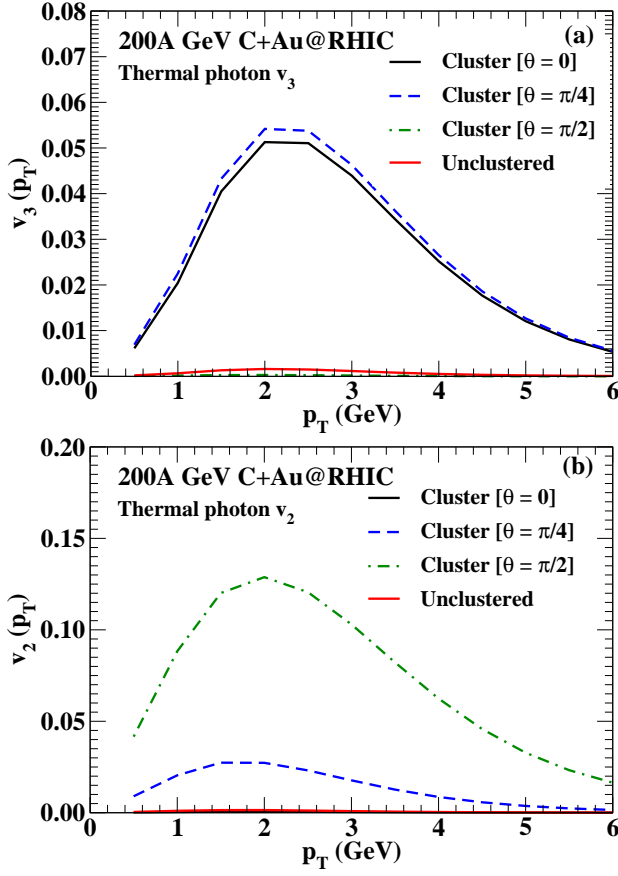


FIG. 5: (Color online) (a) Triangular and (b) elliptic flow of thermal photons as a function of p_T from different configuration of clustered C and Au collisions at 200A GeV.

hadronic photon v_3 for the orientation $\theta = 0$ is larger compared to the same obtained at the orientation $\theta = \pi/4$. The reason can be understood from Fig. 2, where we see that the triangular geometry associated with the hottest region is more prominent in Fig 2(b) compared to Fig. 2(a). Whereas, the boundary region, which is the source of hadronic photons, has a larger triangular geometry as shown in Fig. 2(a) compared to Fig. 2(b). The contributions of thermal photon v_2 for the clustered case with the orientation angle $\theta = \pi/2$ are plotted in Fig. 6(b), and we see a similar response. The peak value of the thermal photon v_2 from the QGP phase is found to be about 90% of the peak value of the total thermal photon v_2 and identically, it reflects that the most of the net thermal photon v_2 has built up during the early phase of QGP evolution.

It is to be noted that the value of T_f is fixed for Au+Au collisions by reproducing the experimental data of charged particle spectra and anisotropic flow parameters. We can not do the same for C+Au collisions due to the unavailability of experimental data. Therefore, we use the same T_f for C+Au collisions as in Au+Au collisions. A smaller T_f would enhance the photon yield

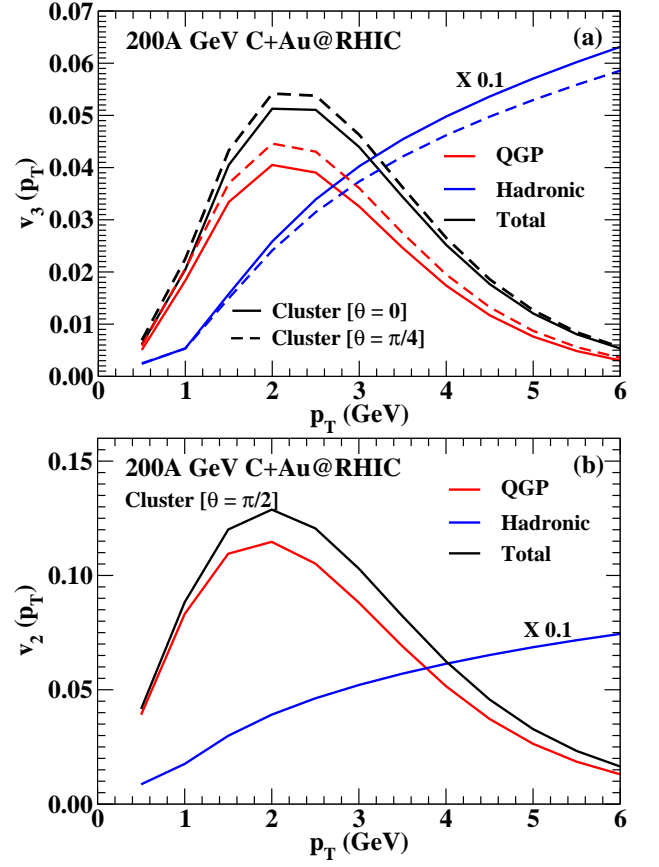


FIG. 6: (Color online) The QGP and hadronic phase contributions of (a) thermal photon $v_3(p_T)$ for the orientation angle $\theta = 0$ and $\pi/4$ (b) thermal photon $v_2(p_T)$ for the orientation angle $\theta = \pi/2$.

from the hadronic phase in the region $p_T < 1$ GeV and the larger p_T part of the direct photon spectrum will remain unaltered. However, the photon anisotropic flow is expected to be larger for a smaller T_f . To show the effect of a relatively longer hadronic phase evolution on the photon flow observables we have calculated thermal photon v_2 and v_3 considering an arbitrary small T_f ($= 120$ MeV, see Fig. 7) for orientation angles $\pi/2$ and $\pi/4$ respectively where, the flow coefficients are estimated to be largest. We see that v_2 and v_3 are enhanced for a smaller T_f , however, the qualitative difference between the photon anisotropic flow parameters remains unchanged even for a significant change in the value of the freeze-out temperature. A detailed study considering a larger formation time and dynamical freeze-out would be valuable in this regards and we postpone it for the future.

The anisotropic flow parameters of direct photons for the clustered configurations with the largest thermal photon v_2 and v_3 are shown in Fig. 8. By ‘direct photons’ we mean the combined contribution of thermal and the prompt photons (produced in initial hard scatterings). We find that the values of the anisotropic flow coefficients

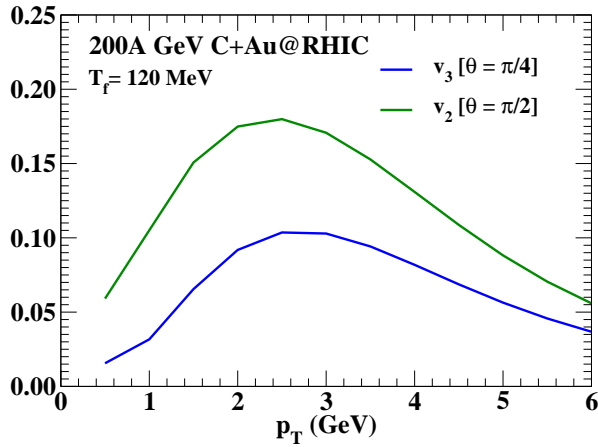


FIG. 7: (Color online) The thermal photon v_3 and v_2 from the clustered C and Au collisions at 200A GeV with orientation angles $\theta = \pi/4$ and $\pi/2$ respectively for $T_f = 120$ MeV.

are substantially large even after inclusion of the prompt contribution (The prompt spectrum is generated in the region $p_T > 2$ GeV (due to some constraints) using JET-PHOX and as a result we could not show the anisotropic flow in the low p_T region). The maximum value of direct photon v_3 and v_2 (at 2 GeV) are found to be about 70% of their respective maximum thermal photon v_3 and v_2 values. It is to be noted that these values are comparable to the anisotropic flow parameter data obtained from the 0 – 20% Au+Au and Pb+Pb collisions at RHIC and LHC energy respectively [62, 63]. Thus, considering even a smooth initial condition, we can obtain a significantly large direct photon v_2 and v_3 depending upon the orientations of collision for the clustered carbon. We expect that the inclusion of initial state fluctuations would further increase the value of direct photon v_2 and v_3 . On the other hand, photon v_2 and v_3 for unclustered carbon appear only due to initial state fluctuations and are expected to be significantly smaller than the clustered carbon. Thus, the clustered carbon and gold collisions at the RHIC have the potential to produce considerably large anisotropic flow parameters of photons even for the most central events. Furthermore, the strong sensitivity of the anisotropic flow parameters to the initial geometry and early QGP evolution also can be valuable to understand the ‘direct photon puzzle’. Our main focus in the present calculation is only to estimate the effect of initial geometry on the production and anisotropic flow parameters of photons. A more realistic calculation, using an event-by-event (3+1) dimensional hydrodynamic framework, would be valuable to precisely explore the role of fluctuations and participant asymmetry on the evolution of thermodynamic quantities and anisotropic flow parameters of photons.

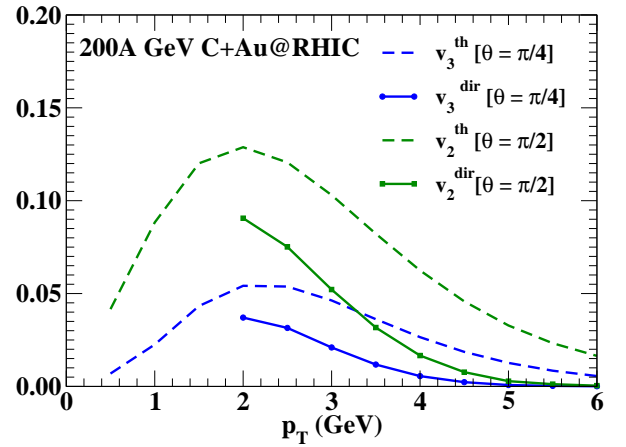


FIG. 8: (Color online) The direct photon v_3 and v_2 from the clustered C and Au collisions at 200A GeV with orientation angles $\theta = \pi/4$ and $\pi/2$ respectively.

D. Geometry (flow) correlation

To get an idea of the experimental signature, we simulate a large number of clustered C+Au events with different configurations and compare the results obtained from the collisions of unclustered carbon. Fig. 9 shows the average orientation angle $\langle\theta\rangle$ as a function of the number of participants in the collisions of clustered carbon, where and henceforth $\langle...\rangle$ denotes an event average. We observe that with the increasing N_{part} , the average angle reduces significantly. Thus, based on the multiplicity cut, it may be possible to select events with various configurations.

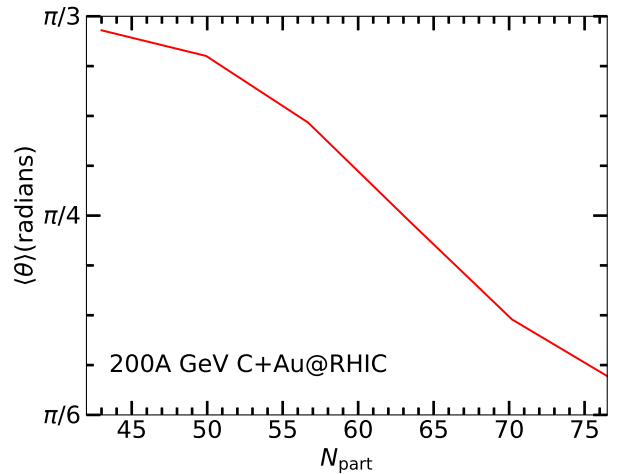


FIG. 9: (Color Online) Average orientation angle $\langle\theta\rangle$ as a function of N_{part} for α -clustered C + Au collisions at 200A GeV.

In Fig. 10(a) we present the N_{part} dependence of average eccentricity and triangularity in unclustered and α -clustered C + Au collisions at 200A GeV. We consider

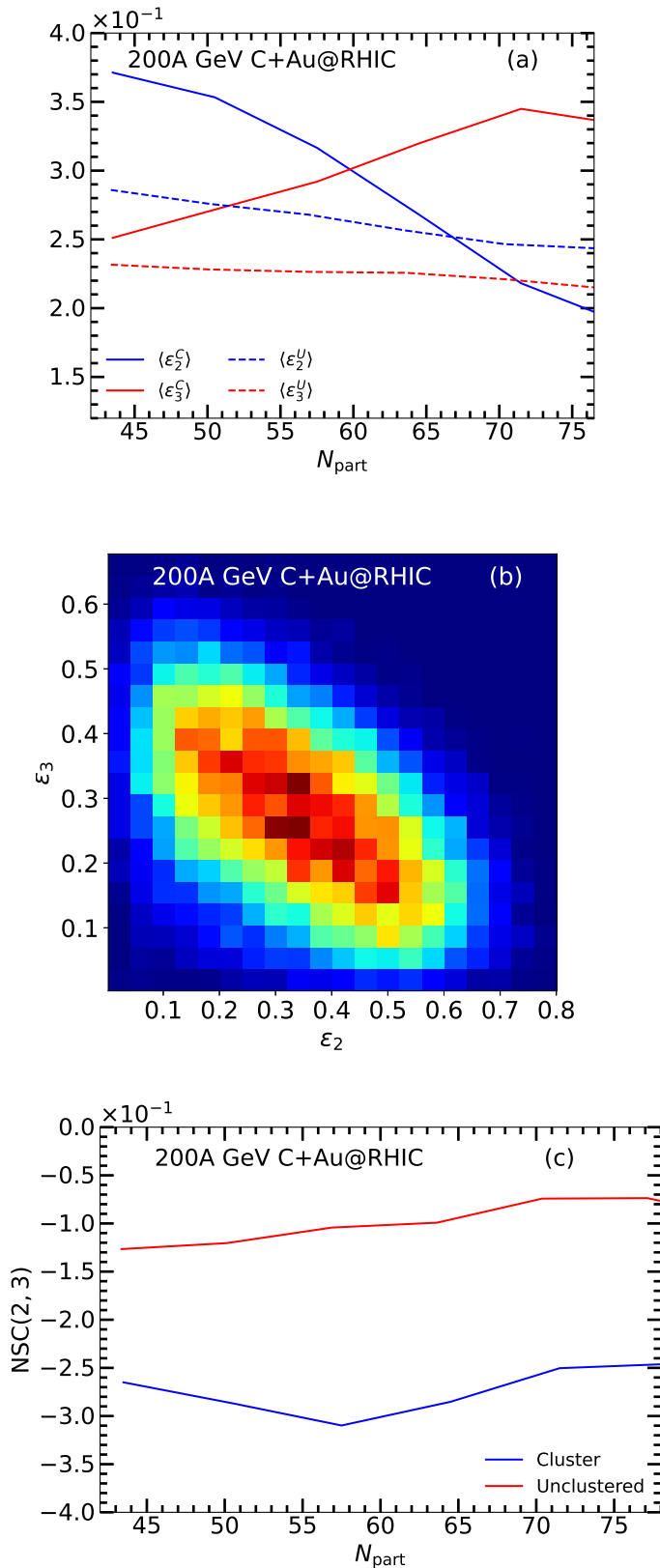


FIG. 10: (Color Online) (a) The average ellipticity and triangularity as a function of N_{part} for α -clustered and unclustered C+ Au collisions at 200A GeV (b) Event distribution in $\epsilon_2 - \epsilon_3$ plane and (c) The normalized symmetric cumulants $\text{NSC}(2,3)$ as functions of N_{part} for unclustered and α -clustered cases. The events are chosen with $N_{\text{part}} > 40$.

the events having $N_{\text{part}} > 40$. The superscripts ‘U’ and ‘C’ stand for the unclustered and clustered carbon respectively. We see that $\langle \epsilon_2^U \rangle$ and $\langle \epsilon_3^U \rangle$ show similar behavior with increasing N_{part} . Due to vanishing geometric deformation and smaller fluctuations at a larger N_{part} , the average eccentricity decreases. We observe a different trend for clustered carbon. Due to the intrinsic triangular geometry of the clustered-carbon, $\langle \epsilon_3^C \rangle$ increases with N_{part} , whereas $\langle \epsilon_2^C \rangle$ decreases. The difference becomes substantial at larger N_{part} , which indicates an obvious anti-correlation between ellipticity and triangularity exists in α -clustered C + Au collisions.

In Fig. 10(b) we plot the event density distribution in $\epsilon_2 - \epsilon_3$ plane for the collisions of clustered carbon. To quantify the anti-correlation, we define a normalized symmetric cumulants coefficient $\text{NSC}(n,m)$ as follows [80],

$$\text{NSC}(n,m) = \frac{\langle \epsilon_n^2 \epsilon_m^2 \rangle - \langle \epsilon_n^2 \rangle \langle \epsilon_m^2 \rangle}{\langle \epsilon_m^2 \rangle \langle \epsilon_n^2 \rangle}. \quad (9)$$

The $\text{NSC}(2,3)$ is expected to be similar to the quantity involving the anisotropic flow coefficients (v_2 and v_3) under a linear response assumption [81, 82]. In Fig. 10(c), we show the normalized symmetric cumulants coefficient as function of N_{part} for both unclustered and α -clustered cases. The negative values of coefficients signify the anti-correlation relation between the two variables. We see a larger anti-correlation for the clustered case compared to the unclustered case. The coefficients for both the cases do not show significant N_{part} dependence. The $\text{NSC}(2,3)$ for the clustered carbon is found to be three times larger than the $\text{NSC}(2,3)$ obtained for the unclustered carbon. We find a small minimum of $\text{NSC}(2,3)$ at $N_{\text{part}} \sim 57$, where the values of the $\langle \epsilon_2^C \rangle$ and $\langle \epsilon_3^C \rangle$ are close to each other. Exploring the large anti-correlation between ellipticity and triangularity (elliptic flow and triangular flow), we can detect the α -cluster effects of carbon in C + Au collisions. It is to be noted that some earlier studies have explored the characteristics of the initial-state eccentricities and final hadron flow observables from the collisions of the clustered carbon and heavy-ions at various beam energies in the event-by-event framework [28, 30]. In principle, we expect that the anti-correlation behavior should hold for both photons and hadrons, since their flow observables basically arise from the initial geometry.

V. SUMMARY

We have calculated p_T spectra and differential anisotropic flow coefficients of thermal photons for α -clustered C and Au collisions at RHIC using a hydrodynamic model with the event-averaged smooth initial density distribution and compared the results with those obtained from unclustered carbon and gold collisions. Three different orientations of collision for the α -clustered carbon have been considered which produce

notably different initial spatial ellipticities and triangularities.

The slope of the thermal photon spectrum depends on the orientation of collision. A larger initial temperature for the orientation angle $\theta = \pi/2$ results in more high p_T photons from the early stage of system evolution compared to the other configurations. However, we see no significant difference in the direct photon spectra for various configurations due to the large contribution of prompt photons in the region $p_T > 3$ GeV. We see significantly large thermal photon v_2 and v_3 from the configurations $\theta = \pi/2$ and $\theta = 0, \pi/4$ respectively, which are large and comparable to the experimental data of photon v_2 and v_3 from the mid-central 200A GeV Au+Au collisions at RHIC. On the other hand, photon v_2 and v_3 from the unclustered C + Au collisions are close to zero as the corresponding spatial anisotropies are vanishingly small for the system. We find that addition of the prompt photon contribution dilutes the anisotropic flow parameters but still their values are substantially larger in comparison to the theoretical estimate of anisotropic flow parameters of direct photons obtained for the mid-central Au+Au collisions. We have studied the individual contributions of the thermal photon v_2 and v_3 from QGP and hadronic phases and have found that these anisotropic flow coefficients are predominantly built during the QGP evolution. As the effect of viscosity which prolongs the evolution of

the QGP is not included here, we expect that it could change the magnitude but not the qualitative nature of these photon observables. Thus, we find that anisotropic flow of photons from the clustered carbon are sensitive to the anisotropic nuclear distribution of C and can potentially help us to understand the photon v_n puzzle. A strong anti-correlation between ellipticity and triangularity is observed because of the exotic internal structure of α -clustered carbon. With the aid of these special features of photon spectra and anisotropic flows, it could be a potential probe to detect the exotic internal structure of α -clustered carbon in the future high energy C + Au experiment.

Acknowledgments

This work is supported by the National Natural Science Foundation of China under Grants No. 11835002, No. 11890710, No. 11890714, No. 11975079 and No. 11961131011, the Strategic Priority Research Program of Chinese Academy of Sciences under Grant No. XDB34030000, Shanghai Pujiang Program under Grant No. 19PJ1401400, and the Guangdong Major Project of Basic and Applied Basic Research under Grant No. 2020B0301030008.

-
- [1] F. G. Gardim, G. Giacalone, M. Luzum and J. Y. Ollitrault, *Nature Phys.* **16**, no.6, 615-619 (2020).
 - [2] S. S. Adler *et al.* [PHENIX], *Phys. Rev. Lett.* **91**, 182301 (2003).
 - [3] B. Alver and G. Roland, *Phys. Rev. C* **81**, 054905 (2010).
 - [4] K. Aamodt *et al.* [ALICE], *Phys. Rev. Lett.* **105**, 252302 (2010).
 - [5] J. Chen, D. Keane, Y. G. Ma, A. Tang and Z. Xu, *Phys. Rept.* **760**, 1 (2018).
 - [6] P. F. Kolb and U. W. Heinz, [nucl-th/0305084].
 - [7] P. Huovinen, [nucl-th/0305064].
 - [8] P. F. Kolb, J. Sollfrank and U. W. Heinz, *Phys. Rev. C* **62**, 054909 (2000).
 - [9] D. Teaney, J. Lauret and E. V. Shuryak, nucl-th/0110037.
 - [10] P. Huovinen and P. V. Ruuskanen, *Ann. Rev. Nucl. Part. Sci.* **56**, 163 (2006).
 - [11] P. Romatschke and U. Romatschke, *Phys. Rev. Lett.* **99**, 172301 (2007).
 - [12] D. A. Teaney, *Quark-Gluon Plasma 4*, 207 (2010).
 - [13] L. Yan, *Chin. Phys. C* **42**, 042001 (2018).
 - [14] H. Holopainen, H. Niemi and K. J. Eskola, *Phys. Rev. C* **83**, 034901 (2011).
 - [15] B. Schenke, P. Tribedy and R. Venugopalan, *Phys. Rev. Lett.* **108**, 252301 (2012).
 - [16] U. Heinz, Z. Qiu and C. Shen, *Phys. Rev. C* **87**, no.3, 034913 (2013).
 - [17] C. E. Coleman-Smith, H. Petersen and R. L. Wolpert, *J. Phys. G* **40**, 095103 (2013).
 - [18] P. Sorensen, *J. Phys. G* **37**, 094011 (2010).
 - [19] J. Takahashi, B. M. Tavares, W. L. Qian, R. Andrade, F. Grassi, Y. Hama, T. Kodama and N. Xu, *Phys. Rev. Lett.* **103**, 242301 (2009).
 - [20] U. W. Heinz and A. Kuhlman, *Phys. Rev. Lett.* **94**, 132301 (2005).
 - [21] M. Rybczynski, W. Broniowski and G. Stefanek, *Phys. Rev. C* **87**, no.4, 044908 (2013).
 - [22] Q. Y. Shou, Y. G. Ma, P. Sorensen, A. H. Tang, F. Videbak and H. Wang, *Phys. Lett. B* **749**, 215-220 (2015).
 - [23] X. G. Cao, G. Q. Zhang, X. Z. Cai, Y. G. Ma, W. Guo, J. G. Chen, W. D. Tian, D. Q. Fang and H. W. Wang, *Phys. Rev. C* **81**, 061603 (2010).
 - [24] U. W. Heinz and J. S. Moreland, *J. Phys. Conf. Ser.* **1271**, 012018 (2019).
 - [25] C. Aidala *et al.* [PHENIX], *Nature Phys.* **15**, no.3, 214-220 (2019).
 - [26] Y. Liu and Y. L. Ye, *Nucl. Sci. Tech.* **29**, 184 (2018).
 - [27] J. -P. Ebran, E. Khan, T. Nikšić and D. Vretenar, *Nature* **487**, 341-344 (2012).
 - [28] W. Broniowski and E. Ruiz Arriola, *Phys. Rev. Lett.* **112**, no.11, 112501 (2014).
 - [29] M. Rybczynski, M. Piotrowska and W. Broniowski, *Phys. Rev. C* **97**, no.3, 034912 (2018).
 - [30] P. Bozek, W. Broniowski, E. Ruiz Arriola and M. Rybczynski, *Phys. Rev. C* **90**, no.6, 064902 (2014).
 - [31] G. Gamow, *Constitution of atomic nuclei and radioactivity*, p. 50 (Clarendon Press, Oxford, 1931).
 - [32] F. Hoyle, *Astrophys. J. Suppl.* **1**, 121-146 (1954).
 - [33] C. W. Cook, W. A. Fowler, C. C. Lauritsen and T. Lauritsen, *Phys. Rev.* **107**, 508-515 (1957).

- [34] R. Roth, S. Binder, K. Vobig, A. Calci, J. Langhammer and P. Navratil, Phys. Rev. Lett. **109**, 052501 (2012).
- [35] M. Chernykh, H. Feldmeier, T. Neff, P. von Neumann-Cosel and A. Richter, Phys. Rev. Lett. **98**, 032501 (2007).
- [36] S. C. Pieper, K. Varga and R. B. Wiringa, Phys. Rev. C **66**, 044310 (2002).
- [37] A. Tohsaki, H. Horiuchi, P. Schuck and G. Ropke, Phys. Rev. Lett. **87**, 192501 (2001).
- [38] Y. Funaki, A. Tohsaki, H. Horiuchi, P. Schuck and G. Ropke, Phys. Rev. C **67**, 051306 (2003).
- [39] Y. Funaki, A. Tohsaki, H. Horiuchi, P. Schuck and G. Ropke, Eur. Phys. J. A **28**, 259-263 (2006).
- [40] W. He, Y. G. Ma, X. Cao, X. Cai and G. Zhang, Phys. Rev. Lett. **113**, 032506 (2014).
- [41] W. He, Y. G. Ma, X. Cao, X. Cai and G. Zhang, Phys. Rev. C **94**, 014301 (2016).
- [42] B. Huang, Y. G. Ma and W. He, Phys. Rev. C **95**, 034606 (2017).
- [43] B. S. Huang, Y. G. Ma and W. B. He, Eur. Phys. J. A **53**, 119 (2017).
- [44] B. S. Huang and Y. G. Ma, Phys. Rev. C **101**, no.3, 034615 (2020).
- [45] S. Zhang, Y. G. Ma, J. Chen, W. He and C. Zhong, Phys. Rev. C **95**, 064904 (2017).
- [46] S. Zhang, Y. G. Ma, J. Chen, W. He and C. Zhong, Eur. Phys. J. A **54**, 161 (2018).
- [47] D. K. Srivastava, J. Phys. G **35**, 104026 (2008).
- [48] C. Gale, Y. Hidaka, S. Jeon, S. Lin, J. F. Paquet, R. D. Pisarski, D. Satow, V. V. Skokov and G. Vujanovic, Phys. Rev. Lett. **114**, 072301 (2015).
- [49] R. Chatterjee, H. Holopainen, I. Helenius, T. Renk and K. J. Eskola, Phys. Rev. C **88**, 034901 (2013).
- [50] C. Shen, U. W. Heinz, J. F. Paquet, I. Kozlov and C. Gale, Phys. Rev. C **91**, no.2, 024908 (2015).
- [51] A. Monnai, Phys. Rev. C **90**, no.2, 021901 (2014).
- [52] L. McLerran and B. Schenke, Nucl. Phys. A **929**, 71-82 (2014).
- [53] F. M. Liu and S. X. Liu, Phys. Rev. C **89**, no.3, 034906 (2014).
- [54] G. Basar, D. Kharzeev, D. Kharzeev and V. Skokov, Phys. Rev. Lett. **109**, 202303 (2012).
- [55] K. Tuchin, Phys. Rev. C **87**, no.2, 024912 (2013).
- [56] B. G. Zakharov, Eur. Phys. J. C **76**, no.11, 609 (2016).
- [57] G. Vujanovic, J. F. Paquet, G. S. Denicol, M. Luzum, B. Schenke, S. Jeon and C. Gale, Nucl. Phys. A **932**, 230-234 (2014).
- [58] H. Li, F. Liu, G. L. Ma, X. N. Wang and Y. Zhu, Phys. Rev. Lett. **106**, 012301 (2011).
- [59] G. L. Ma, Phys. Lett. B **724**, 278-282 (2013).
- [60] A. Adare *et al.* [PHENIX], Phys. Rev. Lett. **104**, 132301 (2010).
- [61] J. Adam *et al.* [ALICE], Phys. Lett. B **754**, 235-248 (2016).
- [62] A. Adare *et al.* [PHENIX], Phys. Rev. C **94**, no.6, 064901 (2016).
- [63] S. Acharya *et al.* [ALICE], Phys. Lett. B **789**, 308-322 (2019).
- [64] P. Dasgupta, R. Chatterjee, S. K. Singh and J. E. Alam, Phys. Rev. C **97**, no.3, 034902 (2018).
- [65] C. Shen, Nucl. Part. Phys. Pro. 276?278, 72 (2016) .
- [66] C. Gale, J. F. Paquet, B. Schenke and C. Shen, Nucl. Phys. A **1005**, 121863 (2021).
- [67] I. Iatrakis, E. Kiritsis, C. Shen and D. L. Yang, JHEP **04**, 035 (2017).
- [68] R. Chatterjee, P. Dasgupta and D. K. Srivastava, Phys. Rev. C **96**, no.1, 014911 (2017).
- [69] P. Dasgupta, R. Chatterjee and D. K. Srivastava, Phys. Rev. C **95**, no.6, 064907 (2017).
- [70] P. Dasgupta, R. Chatterjee and D. K. Srivastava, J. Phys. G **47**, no.8, 085101 (2020).
- [71] V. Y. Naboka, Y. M. Sinyukov and G. M. Zinovjev, Phys. Rev. C **97**, no.5, 054907 (2018).
- [72] V. Y. Naboka, Y. M. Sinyukov and G. M. Zinovjev, Nucl. Phys. A **1000**, 121843 (2020).
- [73] K. J. Eskola, H. Honkanen, H. Niemi, P. V. Ruuskanen and S. S. Rasanen, Nucl. Phys. A **774**, 805-808 (2006).
- [74] M. Laine and Y. Schroder, Phys. Rev. D **73**, 085009 (2006).
- [75] P. B. Arnold, G. D. Moore and L. G. Yaffe, JHEP **12**, 009 (2001).
- [76] J. Ghiglieri, J. Hong, A. Kurkela, E. Lu, G. D. Moore and D. Teaney, JHEP **05**, 010 (2013).
- [77] S. Turbide, R. Rapp and C. Gale, Phys. Rev. C **69**, 014903 (2004).
- [78] G. L. Ma and X. N. Wang, Phys. Rev. Lett. **106**, 162301 (2011).
- [79] P. Aurenche, M. Fontannaz, J. P. Guillet, E. Pilon and M. Werlen, Phys. Rev. D **73**, 094007 (2006).
- [80] G. Giacalone, L. Yan, J. Noronha-Hostler and J. Y. Ollitrault, Phys. Rev. C **94**, 014906 (2016).
- [81] J. Noronha-Hostler, L. Yan, F. G. Gardim and J. Y. Ollitrault, Phys. Rev. C **93**, 014909 (2016).
- [82] L. Yan and J. Y. Ollitrault, Phys. Lett. B **744**, 82-87 (2015).